Research Article Vol. 32, No. 20 / 23 Sep 2024 / Optics Express 34777
Optics EXPRESS

A-central model for the geometric calibration of hyper-hemispherical lenses

EMANUELE SIMIONI,[1,*] CLAUDIO PERNECHELE,[1] WOLFGANG ERB,[2] ANDREA MARCHINI,[2] PAOLO MARTINI,[1] LUIGI LESSIO,[1] LUCA PENASA,[1] AND MONICA BEGHINI[3]

[1]*INAF Padua Observatory, 35122 Padua, Italy*
[2]*Università degli Studi di Padova, Dipartimento di Matematica "Tullio Levi-Civita," 35121 Padua, Italy*
[3]*DISMA, Dipartimento di Scienze Matematiche "Giuseppe Luigi Lagrange," 10129 Turin, Italy*
[*]*xyz@optica.org*

Abstract: Hyper-hemispherical lenses are optical objective lenses with an ultra-wide field of view. Due to their extreme field of view, the geometric calibration introduces several setup difficulties. Various methods have been developed for simplifying the geometric calibration of a camera in the close-range field by defining intrinsic and extrinsic calibration parameters in a limited ambience of a clean room and taking advantage of simple calibration chessboards. A well-known example in this regard is Zhang's approach for pinhole cameras. A similar approach was pursued by Scaramuzza to model more extensive cameras that include fisheye and panoramic lenses. However, despite this toolbox's efficiency, it is ineffectual in the case of a hyper-hemispherical lens because of model limitations in the approximation of the corresponding projection system. In this study, we define and validate what we believe to be a novel a-central model extension (AME) for the description of hyper-hemispherical lenses that is able to overcome these limitations and to describe more accurately the physical behavior introduced by the design of these lenses. For this apparently new a-central model, we obtain significantly improved calibration results for one of the cameras designed in our laboratory and planned to become a planetary payload of an ESA mission.

1. Introduction

The hyper hemispherical (HH) lens design offers significant advantages in space applications by providing a much larger field of view (FoV) without the need for moving parts, which is crucial for reliability. Our institute developed an HH lens for a panoramic camera (hereinafter "PANCAM" [1]), reducing the cost, complexity, and weight. This design excels as a star sensor for autonomous attitude determination [2], particularly focusing on star identification algorithms [3] and attitude estimation accuracy, thus enhancing spacecraft efficiency. The specific design of the lens does not allow considering this camera as a single viewpoint omnidirectional projection system, but it requires high accuracy in its geometric calibration given its scientific and photogrammetric purposes.

From and historical point of view, the geometric calibration of HH lenses in controlled environments such as laboratories poses challenges due to their wide FoV, which limits traditional methods such as a two-axis rotator [4], parabolic collimator [5], or hexapod [6]. However, a simplification lies in computer vision techniques, and most notably in Zhang's approach [7,8]. Zhang introduced a robust method that uses simple chessboard targets to model camera projective systems. This technique involves observing a planar pattern at various angles, detecting it, and employing a closed-form solution for initial modeling, which is refined through a maximum likelihood criterion. Zhang's method remains the easiest and most flexible approach. It focuses on the geometric calibration of pinhole cameras and addresses lens distortion without the need for expensive equipment.

#527318 https://doi.org/10.1364/OE.527318
Journal © 2024 Received 12 Apr 2024; revised 10 May 2024; accepted 13 May 2024; published 11 Sep 2024

Optics EXPRESS

The method has been extended by other researchers [9–11] to panoramic lenses; nevertheless, in all the cases considered, the aim of the research was the calibration of panoramic cameras but defined by a single viewpoint omnidirectional projective system; model which cannot be assumed for the PANCAM.

We should underline the recent presence of researches which moved away by the classical idea to optimize a camera model but have shifted to the use of the plenoptic function [12,13] considering the camera a black box but calibrating for each pixel independently the chief ray associated direction and the radiometric sensibility. Even if in the last decade, there has been a lot of progress in using non-parametric camera models for calibration we should consider that differently by a generic imaging model a parametric model can take advantage of the physical design of the instrument as the radial symmetry which can support a global model optimization for a camera like the PANCAM.

The planetary or satellite applications of the camera will require a model, measured on ground but adjustable even after the cruise phase in a not so controlled environment as the one required by plenoptic models.

For these reasons our research was always oriented to a parametric model and the versatility of Zhang approach has led our attention.

Throw the methods developed to extend Zhang approach to panoramic lenses one of the most popular pipelines developed for calibrating fisheye cameras is the MATLAB Computer Vision Toolbox [14], which is based on the OCamCalib package [15]. This package was developed by Scaramuzza [16] and then additively improved, such as in [16].

This research aimed to develop a more comprehensive projection model, expanding on existing approaches such as Zhang's method. Unlike the common pinhole model, this study's focus was on a single viewpoint omnidirectional projective system, which is termed the "central point camera." This system maps the 3D world to sensor space through a virtual reflection surface and orthographic projection, defining an anamorphism with respect to the FoV through Taylor polynomials. While tools like the Scaramuzza toolbox [17] have gained popularity for panoramic and fisheye lenses, they proved to be insufficient for the HH lens in the PANCAM, especially considering its photogrammetric goals. Therefore, this study aims to define a more extensive projection model to include HH lenses as possible targets of the Scaramuzza toolbox expanding its target to no single viewpoint omnidirectional projective systems and allowing the calibration of the PANCAM camera.

The remainder of this paper is organized as follows: Section 2 details the PANCAM camera and its applications, thus providing the motivation for this study; then, Section 3 presents three calibration methods, namely Zhang's method for pinhole cameras, Scaramuzza's method for panoramic lenses, and our team's method, namely the a-central model extension (AME) for HH lenses; next, Section 4 presents the laboratory tests and comparative results of wide-angle projective models; and finally, Section 5 discusses the findings and concludes the study.

2. PANCAM

2.1. Hyper-hemispherical lenses

The HH lenses that we consider had already been designed [1] by our institute. They are part of the very wide-angle class of lenses, which have historically been evaluated for the distortion introduced by the angles of the chief rays from the object side not being preserved when they pass through the optical process of the aperture. The advent of low-cost, large-area digital sensors and faster digital processing have become more widespread in the last decade, making it easier to work on images, often in real time, and to make an undistorted (undeformed) product available to users. The best-known very wide-angle lens is the fisheye lens (1923), which is capable of acquiring a visual field close to the hemispherical range (zenith angle of 180° and azimuth angle of 360°). Omnidirectional lenses [18] are a less used class of very wide-angle lens. In this type

Optics EXPRESS

of camera, the zenith angle can be increased, making the camera able to acquire images even beyond the hemispherical field above and below the horizon. A known limit of such images is the blind zone around the optical axis (zenith angle of almost 0°), which gives the acquired images their famous "donut" shape. The PANCAM camera was designed to combine the functionality of fisheye and omnidirectional lenses with a FoV greater than 180° and to avoid the donut shape by adding two lenses.

A particular HH lens developed by our institute, the PANCAM, considers a design with the following three logical segments: a catadioptric lens for the panoramic field and a lens for the frontal field, both preceding the aperture stop, and an objective lens that is able to image the field on the focal plane. The result (for details, see [1]) is an HH lens capable of avoiding the donut shape, as depicted in Fig. 1:

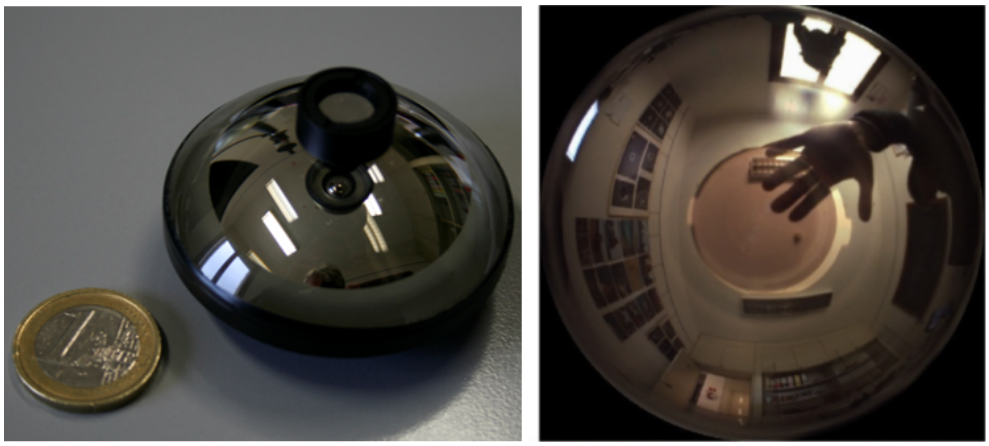

Fig. 1. The HH lens prototype (left) and a "naked" recorded image (right) which shows the not-donut shape of the PANCAM device.

As a point of reference, it is worth mentioning that a fisheye lens covers the range from a zenith angle of 0 to approximately 180°, encompassing the entire horizon. As the Z-field angle (zenithal angle between boresight and extreme FoV) widens, the entrance pupil begins to appear tilted and, once it reaches the extreme angle of 90°, becomes completely darkened. To enable the observation of objects in large Z-fields, the optical designer must adjust the orientation of the entrance pupil. This adjustment can be achieved by moving and compressing the pupil, although there is an associated cost. Instead of the fish eye lenses the optical design of the PANCAM is appropriate for reaching a Z-field angle of 135°.

The frontal field and the huge field of view are the keyframe which have brought the PANCAM the success to different applications as explained in following sections.

Thes work intends to solve a lack in the description of the hyper hemispherical part of the design of the PANCAM, in particular its geometrical definition.

Therefore the frontal field design of the PANCAM is considered marginal to this study which mostly aimed to calibrate the extremely wide FoV of the camera. For this reason, an equivalent design of the lens, deprived of the central components and including only HH lenses is considered from this point forward. Therefore, although the complete PANCAM optical design is the one selected in our main application (see Section 2.3), the geometrical issues, analyzed and solved in this work, all refers to the HH lens which, in any case, represent a not common field of view respect the more commercial cameras.

Through the optical design of these HH lenses, its strength in space applications was already demonstrated [2]. However, the geometric calibration of the more external part of the FoV has

Optics EXPRESS

not achieved a satisfying performance with the more well-known pipeline, which is described in Section 3. The results obtained for calibrating these lenses can be applied to any camera equipped with an extreme field of view.

2.2. PANCAM's optical details

The considered HH lens is based on a specific projection map that is capable of modeling the extreme FoV. The map from the 3D object space to the 2D focal plane can generally be described by the so-called "lens mapping equation," which corresponds to the classical pinhole projection in the case of a narrow lens. As described in [1], the angular field distribution function at the main plane $\psi(Z)$, a function of the zenith angle, is depicted in Fig. 2 for different projective systems.

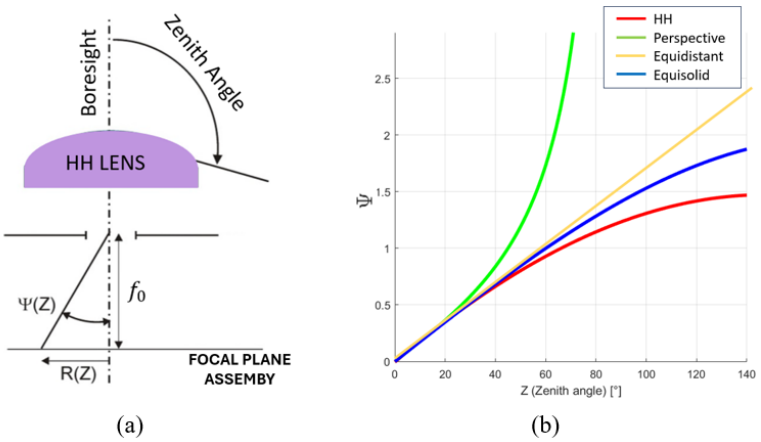

Fig. 2. (a) Functions and parameters included in the projective mapping of a very wide-angle lens; and (b) their trends.

While one can assume a fixed paraxial focal length f_0 in the case of a very wide angle lens, this assumption cannot be made for a pinhole camera because the focal length is dependent on the zenith angle. This dependence generates the deformation of the image along the zenith angle. This deformation can be defined by the relationship between R, the distance of the projected point on the focal plane in respect of the optical axis, and the zenith angle Z.

In particular, the relationship between R (null on the principal point) and the zenith angle (null on the boresight) can be written, for a pinhole camera, as follows:

$$R(Z) = f_0 \tan(Z)$$

While for a fisheye lens, for which the zenith angle can reach 90°, this deformation is easily characterizable, further investigations are required to enable the PANCAM to reach 135°.

Generally, it can be defined as

$$R(Z) = f_0 \Psi(Z)$$

where Ψ is the distribution function and R may have different forms. Some examples of mapping functions are reported in Fig. 2, including equidistant projections (which maintain angular distances due to its linear form) and equisolid ones (which maintain surface relations that subtend an equal solid angle to each pixel).

In the figure above, the vertical asymptote of the perspectives systems is the effect of the fact that the entrance pupil (the pinhole) would be completely obscured for Z = 90°. The most general

Optics EXPRESS

projection function for describing even wide-angle lenses is as follows:

$$R(Z) = f_0 \Psi(Z) = f_0\ k_1 \sin(k_2 Z) \tag{1}$$

This equation describes, for example, the already cited equisolid angle projection ($k_1 = 2$, $k_2 = 0.5$) and the orthographic projection ($k_1 = k_2 = 1$), which maintains planar illuminance. In these projections, the marginal fields are extremely compressed at the focal plane and only make sense for $Z < 90°$.

In [1], as a first approximation, the HH lens was assumed to lie midway between the orthographic and equisolid angle projections; however, considering the singularity of the applications of the lens (described in following section), a more precise definition of the lens was required. This definition had to consider that, as described in the previous section, the enlargement of the FoV for reaching the HH sight introduces an envelope of the entrance pupil, which covers all lens thicknesses, as shown in Fig. 3:

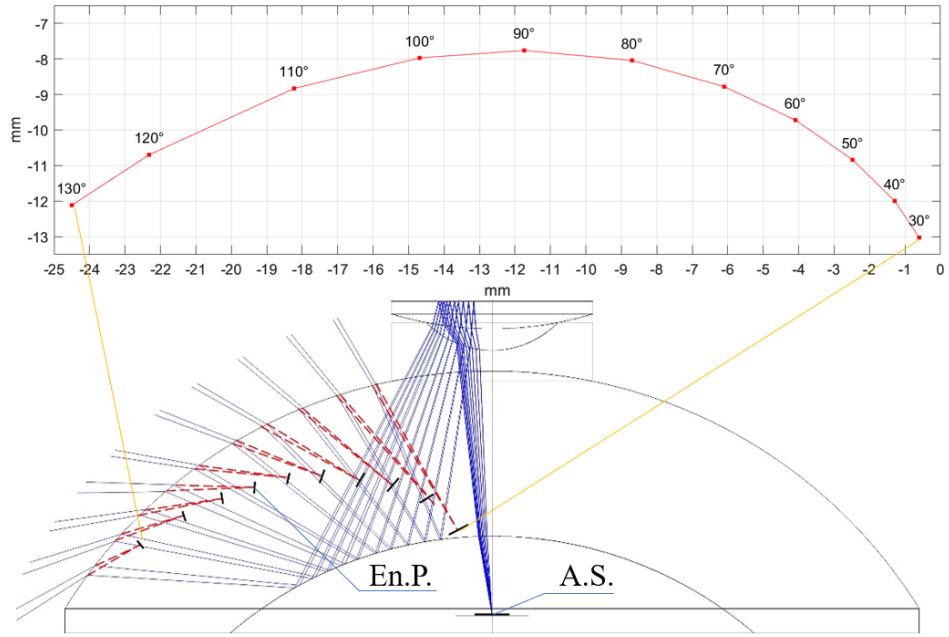

Fig. 3. Two diagrams defined by the Zemax lens project: Top: Entrance pupil movement with a zenith angle from 30° to 130°; bottom: optical path of the chief rays. The image of the aperture stop (A.S.) provides the entrance pupil (En.P.), which is moving and compressing along the field from 30° to 130°. A.S. and En.P.s are indicated by a black thick segment.

Considering a zenith angle that varies between 30° and 130°, the entrance pupil (and thus the viewpoint) moves in a radial direction of more than 20 mm, reaching the limits of the external surface of the lens. At the same zenith angle variation, this corresponds to a vertical (in the boresight direction) movement of 5.27 mm.

The two aforementioned issues (i.e., uncertainty of the projection function and the pupil shift) are the issues that we modeled to extend a well-known calibration toolbox (see Section 3.2) to enable it to be applied to very wide-angle cameras such as the PANCAM as well as to other extremely wide HH cameras.

Optics EXPRESS

2.3. PANCAM's application

The focus of this study was on the HH lenses belonging to PANCAM instrument, which gained significance after the European Space Agency (ESA) launched the Sysnova Lunar Caves Challenge in August 2019. This challenge aimed to gather innovative proposals for exploring and mapping lunar caves or tubes, which have been areas of interest since missions such as Kaguya, LRO, and GRAIL highlighted deep voids beneath the lunar surface [19].

Among the selected proposals, the collaboration between the University of Würzburg, Jacobs University Bremen, the University of Padua, INAF Padua, and VIGEA introduced the DAEDALUS Sphere. This project, which stands for "Descent and Exploration in Deep Autonomy of Lava Underground Structures," aims to explore subsurface voids for potential human habitation.

These lunar caves provide a natural shield from micrometeorites and cosmic rays, with radiation levels at just 0.3% of the lunar surface. Additionally, they offer stable temperatures and possible access to resources such as water. The DAEDALUS mission targets the Marius Hills Hole in Oceanus Procellarum (303.3E, 14.2N), which is believed to lead to a lunar lava tube [19].

For this mission, a highly immersive optical system is crucial. The probe will utilize four PANCAM lenses due to their wide-angle capabilities as well as consider other "simpler" design aspects (i.e., catadioptric [20] or polydioptric [21]). This design ensures that each surface point of the pit will be imaged by at least two cameras, providing redundancy and stereo information.

The use of these HH lenses of the PANCAM allows not only the mapping of the tube but also a photogrammetric approach, which necessitates precise distortion maps or projective systems. This choice was made over other options, namely dioptric and polydioptric systems, due to their temperature sensitivity and complexity, respectively.

In essence, the PANCAM and its HH lenses from our institute [22,23] were selected for their capability to provide comprehensive imaging, redundancy, and stereo information, which is critical for the success of the DAEDALUS mission.

The need for geometric calibration for this purpose has enabled the creation of a model applicable to a generic hyper-hemispherical camera.

3. Overview of projective methods

3.1. Zhang's method

In 2000, Zhang introduced a flexible camera calibration technique [7]. This method involves the camera observing a planar pattern, often a chessboard, from multiple orientations. By detecting the corners of the chessboard, the method estimates intrinsic parameters, distortion, and the plane's positions and orientations. This technique bridges the gap between photogrammetric calibration [20,21], relying on known 3D geometry, and self-calibration [24,25], which involves moving the camera in a static scene. The simplicity of Zhang's method lies in its use of a movable planar surface, allowing for various view orientations.

At the base of the Zhang's algorithm there's a maximum likelihood criterion to estimate camera parameters and extrinsic transformations to minimize the residual of the corners detected. The method's flexibility and accuracy have made it successful, even for satellite instruments [26], offering precise measurements for optical systems approximated as pinhole cameras. In these optical systems, the 3D world points associated with the image coordinates follow the well-known equation in homogenous coordinates:

$$c \sim A\,[R|t]\,X_M \tag{2}$$

where $c \in R^3$ are the homogeneous coordinates of the image point; $X_M \in R^4$ are the 3D homogeneous coordinates in the global reference system; R and t define the roto-translation between the same reference system and the chessboard one; and $A \in R^{3\times3}$ is the intrinsic

Optics EXPRESS

parameters matrix. A includes the main parameters of the projection as the principal point, the instantaneous FoV, and the screw factor [22].

Following updated versions of the toolbox, the optimization allows to define even distortion (assumed as radial and tangential).

Zhang's algorithm, and the ones based on this approach as Scaramuzza one, starting by detecting the m corner using the Harris corner detector [27] and calculates homographies for planar calibration targets that define their X coordinates. Key steps include the following:

1. Images of the pattern are captured from various distances or angles;
2. Tie points are extracted using the Harris corner detector to compute associated homographies;
3. View homographies are used to initially estimate intrinsic parameters with a linear closed-form solution;
4. Chessboard positions and orientations are estimated based on intrinsic parameters;
5. All parameters are refined through nonlinear optimization to minimize residual errors in corner projections.

The last step has the scope of minimizing the residual errors for each corner ($\bar{c}$) defining the projection (P) of all m 3D corners ($\bar{X}$) of all n images acquired through the projective function, which includes the intrinsic and extrinsic parameters defined in (2) and the distortion parameters (d).

The cost function used is the common total square reprojection error:

$$\sum_{i,J=1}^{n,m} \overline{c_{ij}} - P(A, d, R_i, t_i, \overline{X_j})$$

This is a nonlinear minimization problem, which is minimized by the Levenberg–Marquardt (LM) algorithm (see, e.g., [28,29]) and was implemented in [30]. The same approach has then been taken up by more recent researchers to extend the method's application to non-pinhole cameras.

3.2. Scaramuzza's model

Scaramuzza [10] developed a toolbox for estimating projections of fisheye or panoramic images, building on Zhang's algorithm with chessboard images and following the same heuristic described in previous section. Unlike the pinhole model, fisheye lenses have varying instantaneous FoVs, which leads to a toolbox that models projection through a dual system based on a "virtual reflection" that is radially symmetric to the boresight. The mapping of chief rays (see Fig. 4) involves an orthographic projection (O) followed by a central projection (C) based on a Taylor polynomial function.

Figure 4 presents a comparison between the pinhole model (a) and the Scaramuzza model (b). Note that for the Scaramuzza model, the sensor points in an opposite direction in respect of the boresight.

Although the toolbox consider a central projection, prior extensions of MATLAB's Computer Vision Toolbox have addressed axial viewpoint shifts in fisheye lenses; yet, these have been limited to FoVs under 190° [29,31] or, as in the case of [32], the packages were limited to an application to a fisheye lens with an FoV of less than 190° and the simple axial shift is not sufficiently generic for modeling all HH cameras.

Optics EXPRESS

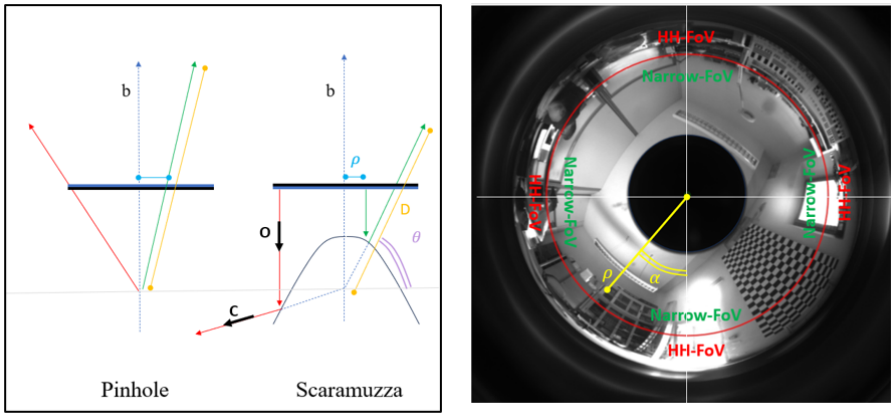

(a) (b)

Fig. 4. In (a) comparison between the pinhole model and the Scaramuzza one with a parallel direction of the boresights (b); In both the cases we show two chief rays belonging to the more external part of the FoV (in red) and to the more narrow (in green). On this chief ray we depicted the most important parameters introduced in the text. In (c) a sample of a PANCAM image, deprived of its frontal field lenses, that define the limits of the green narrow region and the red one belonging to the HH region of the FoV.

Our approach aims to modify and extend the central fisheye model for HH cameras, thereby providing a more comprehensive and generic solution and making the procedure applicable to PANCAM, enhancing its application in photogrammetric and navigation fields.

The panoramic model employs an orthographic projection (O) and a central projection (C), determined by a reflective surface shape described as f, and a zenith angle as a function of the pixel distance from the symmetry axis. Figure 4(a) depicts the boresights, a nominal chief ray (in green), and the outer one (in red) corresponding to the two regions identified in Fig. 4(c). The pinhole model's limitations due to sensor dimensions contrast with Scaramuzza's approach, limited by the reflective shape defined by a Taylor polynomial. If the reflection surface is planar and at a distance equal to the focal length from the principal point, then the model is equivalent.

Although the heuristic use is the Zhang one (described in previous section) in the case of Scaramuzza's toolbox it is applied to a more generic model than a pinhole, allowing representations of a wider range of devices. Intrinsic parameters include the principal point (center of radial distortion), polynomial coefficients that define the virtual reflection surface and an affine transformation for addressing misalignments or astigmatism.

The model's mapping from 3D to 2D coordinates cannot be described by Eq. (2). For panoramic cameras, the azimuth angle's invariance between 3D and 2D is assumed, and mapping the equatorial angle θ (see Fig. 4 in purple) of the chief ray to the resulting distance ρ (see Fig. 4 in light blue) of the projected pixel from the principal point is the focus.

The map can be defined as follows:

$$X = D \begin{bmatrix} \sin\alpha \ \cos\theta \\ \cos\alpha \ \cos\theta \\ \sin\theta \end{bmatrix} \rightarrow m = \rho \begin{bmatrix} \sin\alpha \\ \cos\alpha \end{bmatrix}$$

Optics EXPRESS

Following [10], the relationship between the pixel distance ρ and the equatorial angle θ is defined by the following equation:

$$tan(\theta) = \frac{f(\rho)}{\rho} \tag{3}$$

where the equatorial angle θ is the linear function of the zenith angle ϕ, null on the equator, and it is defined by following equation:

$$\theta = \arctan\left(\frac{z_M}{r_M}\right) = \frac{\pi}{2} - \phi \tag{4}$$

where $r_M = \sqrt{x_M^2 + y_M^2}$ is the distance of the 3D point on the equatorial plane and $[x_M, y_M, z_M]$ are the components of X_M of Eq. (2), which represent the corners' coordinates in mm.

Function f is the function that represents the reflection surface; it is radially symmetric with respect to the optical axis z and should increase monotonically. According to the assumed approximations [10], f is defined as a polynomial of order N, whose coefficients are part of the intrinsic parameters. This polynomial can be seen as a truncated form of the Taylor series $\{a\}_0^N$, which would define the ideal f—that is, the one that perfectly describes the reflection.

The equatorial angle θ corresponds to a chief ray, and the projection on the image can be defined as the smallest ρ, solving Eq. (3), which can be rewritten as follows:

$$a_0 + (a_1 - \tan(\theta))\rho + a_2\rho^2 + \ldots + a_N\rho^N = 0 \tag{5}$$

The minimal root of this equation is the radial distance ρ in pixels. The coordinates of the pixel image associated to the chief ray can be evaluated if one knows the azimuth angle.

Different historical approximations were assumed in the definition of the f function to reduce the number of DoFs. In the traditional Brown distortion model [33], if only even terms are considered, then the final Scaramuzza toolbox does not include a linear term.

The model even optimizes the final affine correction to be applied to the image coordinates to avoid problems linked to mechanical alignments of astigmatism. This correction is approximated with an affine transformation (generally equal to the identity).

The polynomial parameters a_i, affine transformation, and coordinates of the principal point represent the intrinsic parameters measured by the Scaramuzza toolbox.

The time cost of the pipeline is mostly linked to the nonlinear optimization steps, which can take from a few seconds to a few minutes depending on the number of calibration images, the stopping criteria of the LM algorithm, and other factors.

Although the accuracy of this method can generally be compared with that of Harris detection, different results are obtained in the case of an extremely wide-angle camera, as described in the following section.

3.3. A-central model extension

Most existing fisheye models optimized by well-known toolboxes, including MATLAB [14] and OpenCV [29], assume a central projection. However, in practice, cameras equipped with fisheye lenses tend to be axial ones, and this effect is stronger for PANCAM HH lenses. While the entrance pupil moves as the incident ray angle changes in fisheye lenses, causing the apparent viewpoint to shift along the optical axis, this shift cannot be approximated as axial in the case of HH lenses and must be assumed to even be radial, as demonstrated in Section 2.2. Hence, the Scaramuzza method (described in Section 3.2) should not be applied to very wide-angle cameras.

The previous tests performed in our laboratory [34] and the recent described in following sections, indicated that the model described the central part of the FoV well, but that the residuals quickly increased in magnitude moving farther away from the boresight. The highest ones were locally confined to the HH region of the FoV.

Optics EXPRESS

Two assumptions of the Scaramuzza model should be disputed to extend it to a very wide-angle projection system—namely the centrality of the system and the simplicity of the "reflection" surface. Regarding the first problem, it is clear that the model considered in Scaramuzza's approach is central, whereas the envelope of the entrance pupil cannot be considered neglectable in the case of HH lenses, as described in Section 2.2.

Regarding the second problem, projection maps, which generally describe a fisheye or a panoramic camera, can be assumed to be represented by a "virtual reflection" defined by few parameters (fourth-order). In the case of HH lenses, this solution can describe the narrow region of the FoV or the HH region but not both. Various tests have demonstrated that the increase of the order of the polynomials is not generic enough for describing both regions of the FoV. For all the orders, of the Taylor polynomial, between 5 and 7 the residual demonstrated to have standard deviation comparable to the default case of the 4th without a specific decreasing trend. A better solution is the representation of the "virtual reflection" through two different fourth-order Taylor polynomials with a second-order continuity in their separation circle.

For this reason, we divided the FoV into the following two regions, as shown in Fig. 4(c):

1. **Narrow FoV (NF)**: In the NF, Eq. (*7*) can be assumed to be valid.
2. **HH FoV (HF)**: The HF is an external FoV in which the output pupil can be represented as a function of the zenith angle or, more simply, of the distance of the projection from the test.

The two regions can be defined as a thresholding distance in respect of the center of the sensor. We demonstrated this to be optimal at a radial distance of $\rho_s = 700$ pixels, which corresponds to 74.35°, as illustrated in Fig. 4(c).

As explained in the previous section, the Scaramuzza model can be described by Eq. (3) and (4), which can be synthetized as follows:

$$\frac{z_M}{r_M} = \frac{f(\rho)}{\rho} \tag{6}$$

The division of the FoVs was imposed to consider two different functions (f_N and f_{HH}) for respectively describing the NF and HF regions. The narrow field is described here.

As detailed previously, the pipeline minimizes the residuals of the chessboard but supplies no reference fixed point in the 3D world. Thus, if the reference system of the radial component r_M is fixed because it depends on the symmetrical axis, in the case of the z_M, the origin would depend directly on the acquired chessboard.

For this region, the following more generic equation should be considered:

$$\frac{z_M - z_a}{r_M} = \frac{f_N(\rho)}{\rho} \tag{7}$$

where z_a is the position of the pupil in respect to a global reference system. As described previously, this equation assumes a central projection in any case but describes the NF well.

In the case of the HF, we assumed the pupil to be moving along a radial direction and the z axis, as is expected from the lens design (as depicted in Fig. 3). Thus, both the reference systems on the z and r axes can be described as functions of the radial distance ρ.

$$\frac{z_M - z_o(\rho)}{r_M - r_o(\rho)} = \frac{f_{HH}(\rho)}{\rho} \tag{8}$$

Considering the expected movement of the pupil, we assumed a second-order polynomial to define the two functions z_o and r_0. The final model can be described as follows:

$$\begin{cases} \rho < \rho_s \rightarrow & \frac{z_M - z_a}{r_M} = \frac{f_N(\rho)}{\rho} \\ \rho \geq \rho_s \rightarrow & \frac{z_M - (b_0 + b_1\rho + b_2\rho^2)}{r_M - (c_0 + c_1\rho + c_2\rho^2)} = \frac{f_{HH}(\rho)}{\rho} \end{cases}$$

Optics EXPRESS

where

$$\begin{cases} z_0(\rho) = b_0 + b_1\rho + b_2\rho^2 \\ r_0(\rho) = c_0 + c_1\rho + c_2\rho^2 \end{cases} \tag{9}$$

The two FoVs (part of the already considered intrinsic parameters) could be defined by the threshold ρ_s and seven other parameters, including the definition of the two parabolic functions for the HH and the constant height of the pupil (z_a) for the narrow field. Naturally, we could reduce the DoF of this system to three parameters to impose the continuity of the two FoVs.

The ρ_s threshold had to be optimized. As previously mentioned, we obtained better results for this threshold of 700 pixels (the same threshold depicted in Fig. 4(c)), and they were obtained through Newtonian convergency.

Regarding the pupil shift, we assumed second-order continuity on the edge separator of the two fields. Note that this multi-order continuity must be considered in the movement of the pupil defined in Eq. (9); however, this does not imply a continuity of the first order for the map or other derivative products. In any case, by imposing the continuity, we can assume the following:

$$\begin{cases} c_0 = c_2R^2 \\ c_1 = -2\ c_2R \\ b_0 = b_2R^2 + z_a \\ b_1 = -2\ b_2R \end{cases} \tag{10}$$

In the LM regression system [35], various tests have proven the importance of limiting the possible movement of the pupil (in the range of the dimension of the lens) to avoid a wrong local minimum due to the compensation between the pupil shift parameters and the "virtual *reflection*" descriptor polynomial.

Regarding the virtual *reflection*, the NF can be represented by the four Taylor parameters $\{a\}_0^N$ defined in the previous section. By contrast, the HF inherits the same structure, introducing the three remained constraints, namely z_a, b_2, and c_2 (see Eq. ((9)), which can more accurately describe the physical pupil distortion in this extreme region of the FoV.

As described by Eqs. (3) and (5), the narrower region is modeled by the following function:

$$f_N(\rho) = \sum_{i=0}^{4} a_i\rho^i$$

For the HF region, a second function is introduced as follows:

$$g(\rho) = \sum_{i=0}^{4} b_i\rho^i$$

Three constrains are added to maintain the continuity at the limits of the two virtual optical systems:

$$\begin{cases} b_2 = \frac{1}{2}\ddot{f}(\rho_s) - 3b_3\rho_s - 6b_4\rho_s^2 \\ b_1 = \dot{f}(\rho) - 2b_2\rho_s - 3b_3\rho_s^2 - 4b_4\rho_s^3 \\ b_0 = f(\rho) - b_1\rho_s - b_2\rho_s^2 - b_3\rho_s^3 - b_4\rho_s^4 \end{cases}$$

The second and third equations ensure the first-order continuity of the polynomial curve at the limits of the NF and HF fields corresponding to a distance in pixels of ρ_s. The first equation guarantees the continuity at first orders even for an instantaneous FoV.

Optics EXPRESS

The heuristic presented in Section 3.1 can be optimized considering a first estimation of the AME, followed by a refinement using the polynomial approach. This leads to the following heuristics:

- A first extrinsic estimator considering the Scaramuzza approach, identifying a first approximation of the position and orientation of the chessboards;
- A first intrinsic estimator considering the AME, refining the parameters of the camera model identified by Scaramuzza's calibration and adding the new components to describe the pupil shift.
- A first intrinsic estimator considering the AME, refining the parameters of the camera model identified by the previous model and optimizing the virtual reflection extension;
- Multiple iterations of subsequent phases:
  - Extrinsic refinement;
  - Intrinsic refinement (AME).

In the second step (i.e., the first intrinsic estimation), it is assumed that the state vector of the LM optimization has the same calibration parameter values described by Scaramuzza et al. in [10].

The pipeline converges to the best solution, which minimizes the residual reprojection that identifies the chessboard positions and orientations, the polynomial parameters that describe the virtual reflection(both for the narrow and hyper hemispherical regions), the model of the shift of the pupil, and the affine transformation to accommodate the focal plane.

The test, performed in our laboratory, demonstrated that the improvement in the accuracy achieved by using the proposed modifications of the model—with the extension to the non-central projection and the extension of the virtual reflection—can be quite significant.

4. Tests and validations

4.1. Image dataset

The Scaramuzza model and toolbox were previously applied to characterize the PANCAM hyper-hemispheric lenses [34] without completely satisfying results being obtained; for this reason, a more deep/complete analysis was performed.

This work demonstrated the application of the method to a data set of images acquired in our laboratory. The data set covered all FoVs but took advantage of the acquisition of a chessboard of 7×10 squares acquired in 60 poses. The chessboards were printed on panels with a dimension of 10×10 cm for each square. The number of acquisitions was chosen to cover all FoVs in both the azimuthal and zenithal directions.

The images acquisition had the disadvantage of needing manual orientation adjustments to cover all FoVs; however, for convenience, this goal could be achieved by taking advantage of a rotator as the mounting base of the camera to cover all azimuth angles. Some examples of the chessboard images acquired are shown in following sections.

4.2. Results from using the Scaramuzza method

The calibration set of images, described in the previous section, was used to perform the geometric calibration of the HH lens following the classical Scaramuzza pipeline described in Section 3.2.

The resulting coherence of the model and the accuracy of the measured projection were underlined by the residuals, which were defined as the vector differences between the coordinates of the corners detected by the tie point extractor and the ones reprojected through Scaramuzza's model estimated by the pipeline.

Optics EXPRESS

Figure 5 presents reprojections of the corners after the Scaramuzza model's optimization. The detected points are identified by crosses and the reprojections by circles; on the right, the resulting positions and orientations of all the chessboards in the tests are shown.

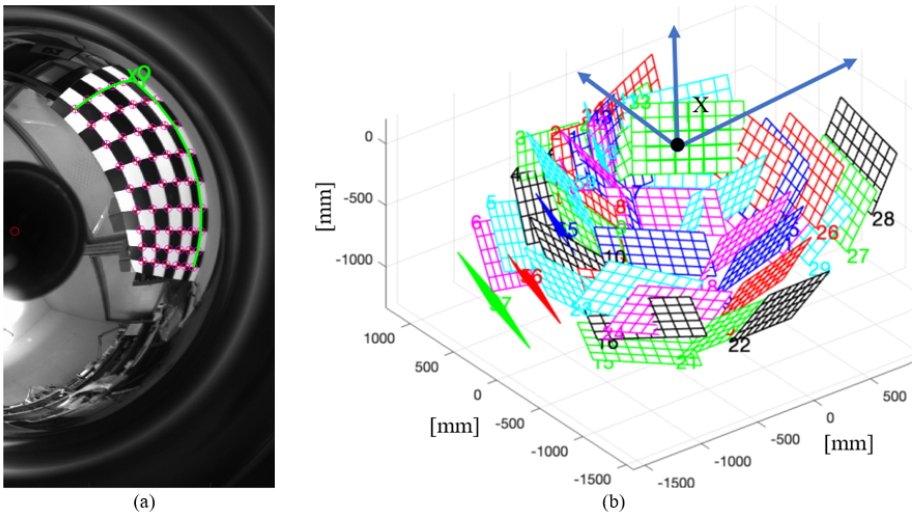

Fig. 5. In (b) an example of the reprojections of the corners (in purple) and the resulting esteemed reference system of the chess board (in green). In (b) and the estimated extrinsic parameters which define the position and the orientation of each chessboard respect the reference system of the camera (X).

The algorithm was able to optimize the camera model described by the two coordinates of the principal point, the five parameters of the polynomial model for the virtual reflection, and the five parameters of the affine transformation.

A summary of the distribution of errors is presented in Fig. 5 for the whole set of images acquired. An average error of 0.824 pixels was measured as being distributed along rows with a standard deviation of 0.62 px and along columns with a standard deviation of 0.58 px.

Although these mean errors seem comparable with the detection error, their distribution along the zenith angle demonstrates the limits of the model. A deeper investigation was performed to correlate the errors introduced by the Scaramuzza model with the projection of each chief ray associated with the corners, as depicted in Fig. 6.

Figure 6(a) depicts the components of the residuals (of all the chessboards acquired) on the line and column of the sensor. In both cases, the Scaramuzza model fit the narrow part of the FoV well, while most of the errors were associated with the high zenith angle, which corresponded to the HF region of the FoV. The same idea is demonstrated in Fig. 6(b), where each corner is identified by a circle with the same dimension of the error (scaled by a factor of 20) and with a linear colormap between the minim and maximum errors obtained. The image underlines the localization of the greater errors in the HF region.

Figure 7 presents two examples of two enlarged regions of images covering the HF region, where the reprojected corners (green circles) are not coherent with those depicted by the image detection (red crosses).

A summary of the calibration measurements is reported in Fig. *8*:

The image shows, in blue (the left y-axis), a map between the pixels (radially considered) and the associated zenith angle, while in red (the right y-axis) it shows the instantaneous FoV associated with each direction.

Optics EXPRESS

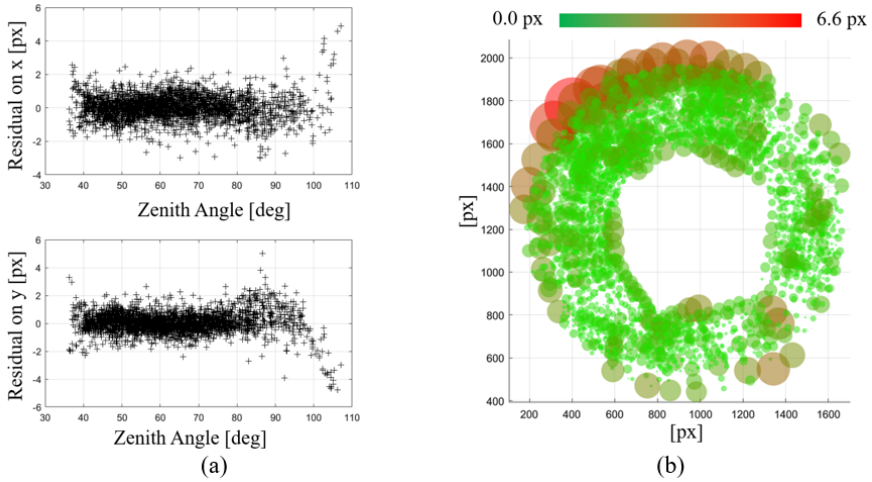

Fig. 6. (a) Distribution of the residual error on the x-axis (top) and the y-axis (bottom) (in respect of the chief ray zenith angle) applying the Scaramuzza model (b) Errors of reprojections associated to each corner for all the images of the test on the sensor plane.

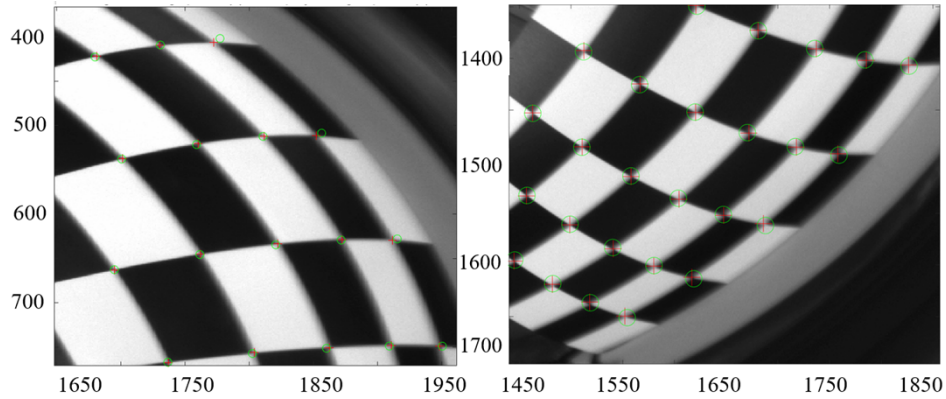

Fig. 7. Details for the HF region of the reprojection (in green) by the Scaramuzza model compared to the detection ponints (in red).

Regarding the trend of the instantaneous FOV, it does not physically represent the correct projection of the HF region. The measurements are in line with previous tests that used the Scaramuzza model applied to an HH lens [34]. Different tests were performed to determine whether an increase in the number of polynomial coefficients could solve the problem without a positive response. Until the 7^{th} order, the results are comparable to the default case of the 4^{th} one. The assumption explained in Section 3.3 avoids the issues that would invalidate the correct solution without losing the generality of the method.

4.3. Results from using the AME

The same investigation that was performed for the Scaramuzza model was applied using the AME, where the camera model was described by the two DoFs of the principal point, the three parameters for the pupil shift, the four parameters of the polynomial model for the narrow region, the two remaining parameters of the polynomial representative for the HF region, and the five

Optics EXPRESS

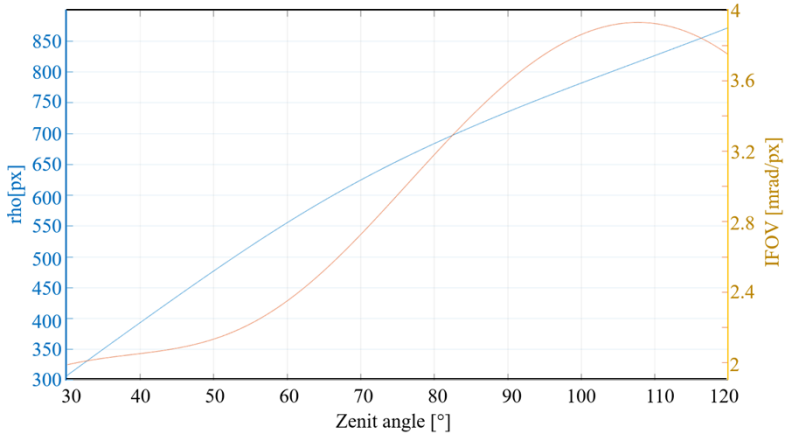

Fig. 8. Summary of the calibration measurements due to the Scaramuzza pipeline showing on the left y axis, in blue, the map between zenith angle and pixel distance from the principal point and, on the right axis, in orange the IFOV measured.

parameters of the affine transformation. The last ones are not reported here because, a part of the numerical noise, could be comparable, in the case of the considered HF region, to identity.

Table 1 reports the results of the optimization of the other parameters, where the mean residual errors are shown for both the two methods considered. They report the mean error and standard deviation of the residual along detector rows (x) and columns (y).

Table 1. Optimized parameters representing the camera model with AME (on the left) and the statistical error in the case of the Scaramuzza model and AME (on the right)

Linear Pupil Coeff				
z_a		b_2	c_2	
0.5122		-1.217e-5	-9.017e-5	
Taylor Polyonomy (4^{th} ord)				
a_0	a_1	a_2	a_3	a_4
-619.543	0	0.0015311	-2.430e-6	2.551e-9
-888.934	-3.8281	0.0229775	-3.731e-5	2.091e-8

Results		
	Scaramuzza	**AME**
Average [px]	0.8237	0.6109
SD x [px]	0.6222	0.5469
SD y [px]	0.5765	0.4888

For an enhanced understanding of the performance of the method and the statistical results reported in Table 1, the same investigation performed for the Scaramuzza model was applied using the AME. Figure 9 depicts the residuals for all of the chessboards as a function of the zenith angle or distributed on the sensor reference system:

Different from the previous images, the trends reveal how the residual errors were invariant in respect of the zenith angle, demonstrating the best fit of the model even for the HF region, which corresponds to high zenith angles. The higher accuracy, although concentrated in the external part of the field, led to a global improvement of more than 20%.

This increase in precision, extendable to the application of this approach to any hyper-hemispherical camera, will have an impact on triangulation following the stereo matching of PANCAM images and therefore on the three-dimensional reconstructions (DTMs) generated from such data.

The same idea is demonstrated by the colored distribution in Fig. 9(b), where each corner is identified by a circle with the same dimension of the error (scaled by a factor of 20) and with a

Optics EXPRESS

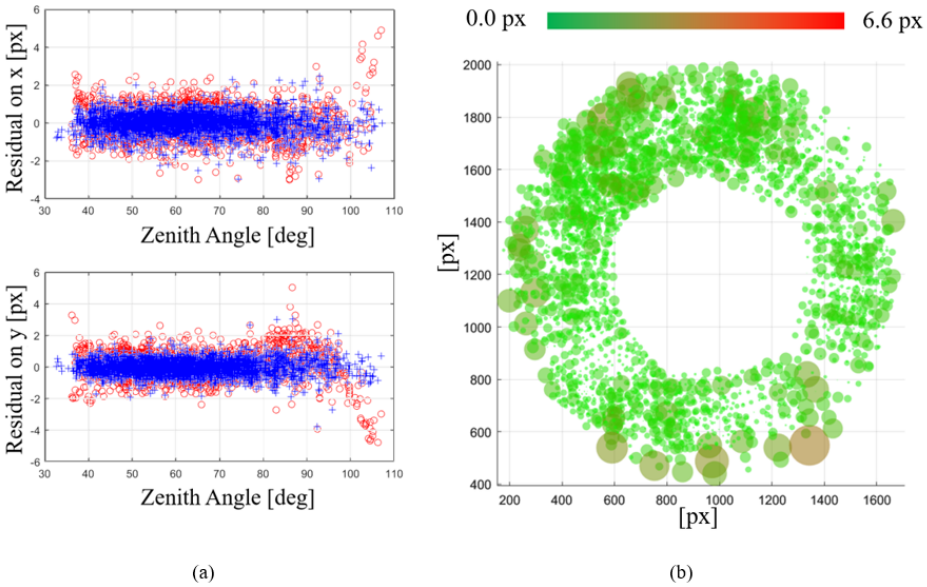

Fig. 9. (a) Distribution of the residual error on the x-axis (top) and the y-axis (bottom) (in respect of the chief ray zenith angle) applying the AME model (blu) compared to Scaramuzza one (red) (b) Errors of reprojections associated to each corner for all the images of the test on the sensor plane.

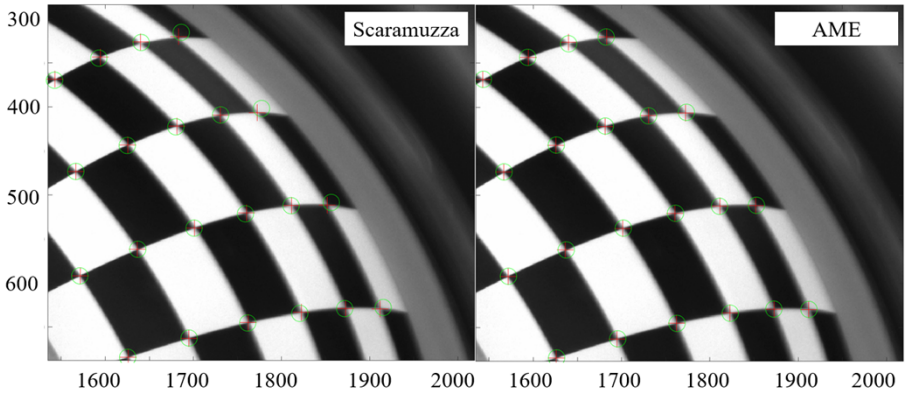

Fig. 10. Comparison of the results obtained by the Scaramuzza pipeline (on the left) and (b) the AME (on the right). Both pictures show the image points as cross and the reprojected point as circles

linear colormap. The color axis range used is the same as those applied in the Scaramuzza model (depicted in Fig. 6).

A comparison of the results obtained using the Scaramuzza pipeline with those obtained using the AME's refinement is presented in Fig. 10. The image presents the detected corners with red crosses and the reprojections as green circles following the two models. In both cases, only a limited part of the image covering the HF region is depicted.

A summary of the calibration measurements is reported for the AME based calibration in Fig. *11*:

Optics EXPRESS

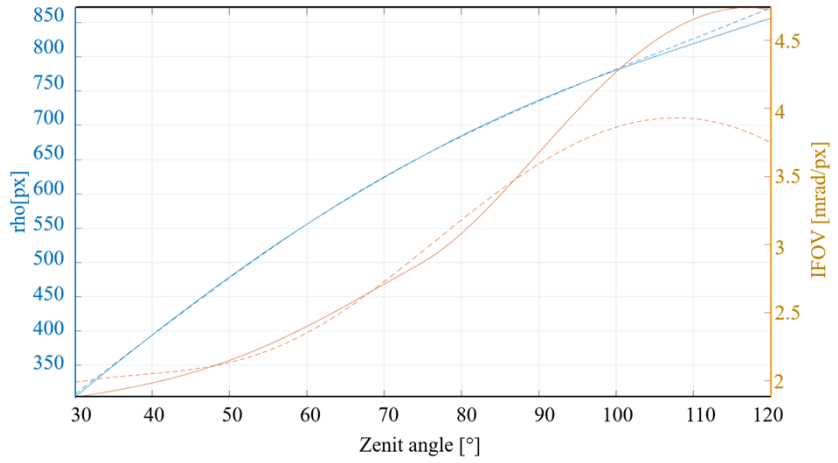

Fig. 11. Summary of the calibration measurements due to the AME pipeline (continuous line) compared to the state of art of Scaramuzza one () showing on the left y axis, in blue, the map between zenith angle and pixel distance from the principal point and, on the right axis, in orange the IFOV measured.

The image presents, in blue, a map between the pixels (radially considered) and the zenith angle associated with each chief ray and, in red, the instantaneous FoV associated with each direction.

The second-order continuity of the instantaneous FOV is an expected result of the separation introduced between the HF and the NF. As explained in Section 4.3, we imposed the second-order continuity of the pupil's position in respect of the chief ray's orientation on the polynomial map's instantaneous FOV. Consequently, the instantaneous FoV is not a linear consequence of this assumption.

5. Conclusion and discussion

This study aimed to propose a solution for applying flexible geometric calibration pipelines, which are currently limited to pinhole fisheye and panoramic cameras, to the broader domain of HH cameras.

The proposed model allows for a seamless transition between the simpler central projection and the more accurate non-central projection, covering a wide range of fisheye designs. Additionally, it extends the capability to define wide-angle cameras, including HH ones that have not been adequately addressed by previous tools.

The focal point of this endeavor was the PANCAM, a dioptric system with an HF up to 135° in the boresight direction. This camera is particularly significant due to its involvement in the recent ESA CDF for Lava Tube Lunar Exploration. The camera was selected to map unexplored lava tubes using both images and stereo pairs. This ambitious goal required an analysis to define a geometric model for its ground-calibrated description and optimization during scientific missions.

The attempt to perform geometric calibration on this type of lens using the Scaramuzza toolbox, the most well-known flexible pipeline for panoramic cameras derived from Zhang's method, highlighted the inefficiency of this model for the HF. These methods inherently assume a central projection as the basis for their heuristics.

This study proposed an extension of the Scaramuzza model named the AME, which is capable of describing a non-central HH projection without introducing an excessive number of DoFs. When the resulting measurements were compared, it became evident that the limitations of the

Optics EXPRESS

Scaramuzza model prevented (see Fig. 8) the measurement of parameters such as the instantaneous FOV in the subequatorial region of the lens.

By contrast, the AME approach, with its robust enhancements, allowed for a flexible and non-constant relationship between the pupil position and zenith angle, accurately describing the expected instantaneous FOV. Once the pipeline had been applied to the calibration images, the AME model could be evaluated. It comprised six parameters for the Taylor polynomials describing the dual reflection, three parameters for describing the movement of the pupil, and an affine transformation.

Upon deriving the intrinsic and extrinsic parameters, the model's accuracy could be assessed by reprojecting corners onto the image and comparing them with the detected corners. The AME demonstrated a 20% reduction in residuals, which are typically strongly distributed in the hyper hemispherical region for the Scaramuzza pipeline, reaching as low as 0.5 pixels (the limit of detection), which thus represents the lower limit of achievable accuracy.

Acknowledgments. Agapi Mou to have supported all this path.

Disclosures. "The authors declare no conflicts of interest."

Data availability. Data underlying the results presented in this paper are not publicly available at this time but may be obtained from the authors upon reasonable request.

References

1. C. Pernechele, "Hyper hemispheric lens," Opt. Express **24**(5), 5014–5019 (2016).
2. C. Pernechele, C. Dionisio, M. Munari, *et al.*, "Hyper hemispheric lens applications in small and micro satellites," Adv. Space Res. **62**(12), 3449–3461 (2018).
3. R. Opromolla, G. Fasano, G. Rufino, *et al.*, "A new star tracker concept for satellite attitude determination based on a multi-purpose panoramic camera," Acta Astronaut. **140**, 166–175 (2017).
4. E. Simioni, V. Da Deppo, C. Re, *et al.*, "SIMBIO-SYS/STC stereo camera calibration: Geometrical distortion," Rev. Sci. Instrum. **90**(4), 043106 (2019).
5. S. Tulyakov, A. Ivanov, N. Thomas, *et al.*, "Geometric calibration of Colour and Stereo Surface imaging system of ESA's Trace Gas Orbiter," Adv. Space Res. **61**(1), 487–496 (2018).
6. J. Rodriguez-Ferreira, F. Poulet, P. Eng, *et al.*, "On-ground calibration of the BEPICOLOMBO/SIMBIO-SYS at instrument level," In *EGU General Assembly Conference Abstracts* (p. 12075) (2012).
7. Z. Zhang, "A flexible new technique for camera calibration," IEEE Trans. Pattern Anal. Machine Intell. **22**(11), 1330–1334 (2000).
8. Z. Zhang, "Flexible camera calibration by viewing a plane from unknown orientations," In *Proceedings of the seventh ieee international conference on computer vision* (Vol. 1, pp. 666–673) (1999).
9. C. Mei and P. Rives, "Single viewpoint omnidirectional camera calibration from planar grids,". In *Proceedings IEEE International Conference on Robotics and Automation* (pp. 3945–3950) (2007).
10. D. Scaramuzza, A. Martinelli, and R. Siegwart, "A flexible technique for accurate omnidirectional camera calibration and structure from motion," In *Fourth IEEE International Conference on Computer Vision Systems (ICVS'06)* (pp. 45) (2006).
11. P. Sturm and S. Ramalingam, "A generic concept for camera calibration," In *Computer Vision-ECCV 2004: 8th European Conference on Computer Vision, Proceedings, Part II 8* (pp. 1–13).(2004).
12. M. D. Grossberg and S. K. Nayar, "A general imaging model and a method for finding its parameters," *Proc. 8th IEEE ICCV 2001, Vancouver, BC, Canada, 2001*, pp. 108-115(2001)
13. S. Ramalingam and P. Sturm, "A Unifying Model for Camera Calibration," in *IEEE Transactions on Pattern Analysis and Machine Intelligence*, vol. 39, no. 7, pp. 1309–1319 (2017).
14. The MathWorks (2024) Fisheye calibration basics. MATLAB documentation, https://www.mathworks.com/help/vision/ug/fisheye-calibrationbasics.html
15. D. Scaramuzza (2024) OCamCalib: Omnidirectional camera calibration toolbox for Matlab, https://sites.google.com/site/scarabotix/ocamcalib-omnidirectional-camera-calibration-toolbox-for-matlab?authuser=0
16. S. Urban, J. Leitloff, and S. Hinz, "Improved wide-angle, fisheye and omnidirectional camera calibration," ISPRS Journal of Photogrammetry and Remote Sensing **108**, 72–79 (2015).
17. J. Y. Bouguet (2022). Camera Calibration Toolbox for Matlab (1.0). CaltechDATA. https://doi.org/10.22002/D1.20164
18. L. H. Kleinschmidt, "Apparatus for producing topographic views," U.S. patent **994**, 935 (1911).
19. J. Haruyama, T. Morota, S. Kobayashi, *et al.*, "Lunar holes and lava tubes as resources for lunar science and exploration. Moon," Prospective Energy and Material Resources 139-163 (2012).
20. Y. Yagi and S. Kawato, "Panorama scene analysis with conic projection,". *IEEE International Conference on Intelligent Robots and Systems, Workshop on Towards a New Frontier of Applications* (1990).

Optics EXPRESS

21. J. Neumann, C. Fermüller, and Y. Aloimonos, "*Polydioptric cameras: New eyes for structure from motion. In Pattern Recognition*," 24th DAGM Symposium Zurich, Proceedings 24 (pp. 618–625). (2002).
22. E. Simioni, V. Da Deppo, Re, *et al.*, "Geometrical distortion calibration of the stereo camera for the BepiColombo mission to Mercury," In *Space Telescopes and Instrumentation* (Vol. 9904, pp. 376–394). SPIE.(2016).
23. E. Simioni, C. Pernechele, R. Pozzobon, *et al.*, "The daedalus cam: the immersive and stereoscopic way for lunar lava tubes esploration," *4th International Planetary Caves Conference 2023* (LPI Contrib. No. 2697), (2023).
24. O. Faugeras, *Three-Dimensional Computer Vision: A Geometric Viewpoint* .MIT Press, (1993).
25. R. Tsai, "A versatile camera calibration technique for high-accuracy 3D machine vision metrology using off-the-shelf TV cameras and lenses," IEEE J. Robot. Automat. **3**(4), 323–344 (1987).
26. E. Simioni, V. Da Deppo, G. Naletto, *et al.*, "*Stereo Camera for satellite application: A new testing method*," IEEE Metrology for Aerospace (MetroAeroSpace) (pp. 582–587). (2014).
27. Konstantinos G. Derpanis, "*The harris corner detector*," York University 2: 1-2. (2004).
28. Andrew Harltey and Andrew. Zisserman, "*Multiple View Geometry in Computer Vision*," Cambridge University Press, 2nd edition. 4, 6 (2006).
29. OpenCV (2024) Fisheye camera model - Camera Calibration and 3D Reconstruction documentation, https://docs.opencv.org/4.x/db/d58/group__calib3d__fisheye.html
30. S. J. Maybank and O. D. Faugeras, "A Theory of Self-Calibration of a Moving Camera," Int'l J. Computer Vision **8**(2), 123–151 (1992).
31. D. Marquardt, "An algorithm for least-squares estimation of nonlinear parameters," SIAM J. Appl. Math. **11**(2), 431–441 (1963).
32. Davide Scaramuzza, A. Martinelli, R. Siegwart, *et al.*, "A toolbox for easily calibrating omnidirectional cameras.," In *IEEE/RSJ International Conference on Intelligent Robots and Systems*, pages 5695–5701 (2006).
33. R. Tezaur, A. Kumar, and O. Nestares, "A new non-central model for fisheye calibration,". In *Proceedings of the IEEE/CVF Conference on Computer Vision and Pattern Recognition* (pp. 5222–5231). (2022).
34. E. Simioni, C. Pernechele, C. Re, *et al.*, "Geometrical calibration for the panrover: A stereo omnidirectional system for planetary rover," Int. Arch. Photogramm. Remote Sens. Spatial Inf. Sci. **XLIII-B3-2020**, 1151–1158 (2020).
35. J. More, *The Levenberg-Marquardt Algorithm, Implementation and Theory Numerical Analysis*," G. A. Watson, eds., Springer-Verlag, (1977).